MOX-Report No. 55/2024

Schwarz Waveform Relaxation and the Unmapped Tent-Pitching Method in 3D

Artoni, A.; Ciaramella, G.; Gander, M.J.; Mazzieri, I.

MOX, Dipartimento di Matematica
Politecnico di Milano, Via Bonardi 9 - 20133 Milano (Italy)

mox-dmat@polimi.it https://mox.polimi.it

Schwarz Waveform Relaxation and the Unmapped Tent-Pitching Method in 3D

Alberto Artoni, Gabriele Ciaramella, Martin J. Gander, and Ilario Mazzieri

1 Introduction

Schwarz Waveform Relaxation (SWR) [6, 5], Mapped Tent Pitching (MTP) [8], and Unmapped Tent Pitching (UTP) [2] are highly efficient algorithms for the space-time parallel solution of hyperbolic problems. Such problems are difficult to solve with other popular Parallel-in-Time (PinT) methods of multilevel type like Parareal and MGRIT, see [7] for a general introduction to PinT methods.

We prove here a new, general equivalence result between MTP and SWR leading to UTP, and present and study UTP for the first time in 3D, applied to a second order wave equation. We prove convergence, and characterize in detail the resulting 4D tent structure. While we present our results for a specific equation, geometry and decomposition, our results also hold in much more general situations.

We consider the 3D second-order wave equation in an open bounded domain $\Omega \subset \mathbb{R}^3$, having regular boundary $\partial\Omega$,

$$\begin{cases} \partial_{tt} u(\mathbf{x}, t) = c^2 \Delta u(\mathbf{x}, t) & \text{for } (\mathbf{x}, t) \in \Omega \times (0, T),\ T > 0, \\ (u, \partial_t u)(\mathbf{x}, 0) = (g_0, g_1)(\mathbf{x}) & \text{for } \mathbf{x} \in \Omega, \\ u(\mathbf{x}, t) = 0 & \text{for } t \in (0, T) \text{ and } \mathbf{x} \in \partial\Omega, \end{cases} \tag{1}$$

where g_0 and g_1 are known functions, and $c > 0$ is the constant wave speed. In what follows, we adhere to the following notation: bold letters denote vectors; vectors in

A. Artoni
MOX, Dipartimento di Matematica, Politecnico di Milano, e-mail: alberto.artoni@polimi.it

G. Ciaramella
MOX, Dipartimento di Matematica, Politecnico di Milano, e-mail: gabriele.ciaramella@polimi.it

M.J. Gander
Section de Mathématiques, Université de Genève, e-mail: martin.gander@unige.ch

I. Mazzieri
MOX, Dipartimento di Matematica, Politecnico di Milano, e-mail: ilario.mazzieri@polimi.it

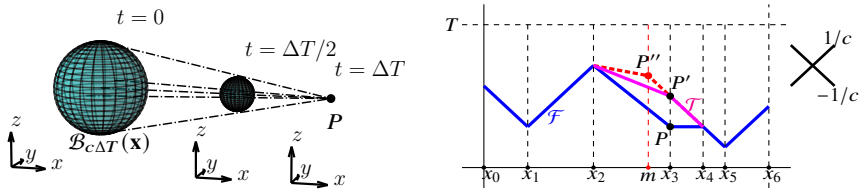

Fig. 1 **Left**: Huygens principle in 3D: the solution at $P = (\mathbf{x}, \Delta T)$ is obtained by the data at $t = 0$ on the closed ball $\mathcal{B}_{c\Delta t}(\mathbf{x})$ of radius $c\Delta T$ and centered in $\mathbf{x}$. **Right**: The dots on the x-axis are the vertices of the 1D grid. The blue line is a computed front $\mathcal{F}$. The magenta line is the tent pitched at P (P is moved along t into P'). The point m is the middle point of the interval/subdomain $\Omega_3 = (x_2, x_4)$. The red dashed line is the volume of computed exact solution by a solve on Ω_3.

$\mathbb{R}^3$ have components denoted by x, y, and z: $\mathbf{x} = (x, y, z)$; calligraphic letters are used for sets: if $\mathcal{A}$ is a set, then $\partial\mathcal{A}$ denotes its boundary; finally, $\mathcal{B}_r(\mathbf{x}) \subset \mathbb{R}^3$ denotes the ball of radius r and center $\mathbf{x}$.

2 MTP and SWR

MTP builds a space-time mesh iteratively by pitching one group of tents after another[1] while solving (1) within the new pitched tents [8]. Since tents generally have complicated geometries, one maps them into space-time cylinders where space and time directions can be separated to apply classical time-stepping schemes. The MTP process begins by assuming that Ω is discretized by a mesh Ω_H, and the iterations are characterized by a so-called *advancing front*: a piecewise-linear and continuous surface, with the same vertices of Ω_H, that bounds in time the volume of the exact or numerically approximated solution. New tents are pitched at each iteration, and (1) is solved within them. The computed solution is hence added to the advancing front, spanning a larger space-time volume. More precisely, the MTP process is obtained by the following steps (see also Fig. 1, right):

1. Consider an already computed front $\mathcal{F}$. At the first iteration $\mathcal{F} = 0$ (a flat surface at $t = 0$).
2. Select a vertex of the mesh Ω_H and the corresponding vertex P on the front $\mathcal{F}$ such that a new tent can be pitched on it.
3. A new point P' is computed by moving P in direction t as long as the exact solution can be computed in P' using the front data on the elements of Ω_H adjacent to P.
4. The new tent $\mathcal{T}$ is defined as the polytope obtained by taking the convex hull of P, P', and the vertices of $\mathcal{F}$ directly connected to P.
5. Solve (1) within $\mathcal{T}$ by a mapping procedure [8].
6. Update the front by adding $\mathcal{T}$ to $\mathcal{F}$.
7. If all vertexes of $\mathcal{F}$ are located at $t = T$ stop, otherwise go to 2.

[1] In classical tent pitching [10], a tent is a space-time finite element, but in MTP it is a generic space-time domain to be discretized, or in which conceptually one could solve exactly.

Notice that step 3 is usually performed using CFL-type conditions based on a finite-difference approximation of the wave-speed coefficient [8]. However, these conditions can be reformulated for constant wave speed as in step 3 above.

SWR is based on an overlapping space decomposition $\Omega = \bigcup_j \Omega_j$. The SWR process is then obtained by iteratively solving subproblems of the form

$$\begin{cases} \partial_{tt} u_j^n(\mathbf{x},t) = c^2 \Delta u_j^n(\mathbf{x},t) & \text{for } (\mathbf{x},t) \in Q_j := \Omega_j \times (0,T), \\ (u_j^n, \partial_t u_j^n)(\mathbf{x},0) = (g_0, g_1)(\mathbf{x}) & \text{for } \mathbf{x} \in \Omega_j, \\ u_j^n(\mathbf{x},t) = 0 & \text{for } t \in (0,T) \text{ and } \mathbf{x} \in \partial\Omega \cap \partial\Omega_j, \\ u_j^n(\mathbf{x},t) = \chi_{j,\ell}(\mathbf{x}) u_\ell^{n-1}(\mathbf{x},t) & \text{for } t \in (0,T),\ \mathbf{x} \in \partial\Omega_j \cap \partial\Omega_\ell, \text{ and } \ell \in \mathcal{N}_j, \end{cases} \tag{2}$$

for $j \in \mathcal{K}_n$. Here, n is the iteration count, $\mathcal{N}_j$ is the set of indices of the subdomains Ω_ℓ intersecting Ω_j, and $\chi_{j,\ell}$ are partition of unity functions, $\chi_{j,\ell}(\mathbf{x}) \geq 0$, with $\sum_\ell \chi_{j,\ell}(\mathbf{x}) = 1$. Moreover, $\mathcal{K}_n$ is the set of indices of the subproblems solved at the n-th iteration. For the parallel SWR the set $\mathcal{K}_n$ contains all subdomain indices.

To draw a general relation between MTP and SWR, we assume that A) the union of the elements adjacent to each vertex of Ω_H is a convex set, and B) each subdomain Ω_j is associated with a vertex P_j of Ω_H and is obtained as the union of all the elements of Ω_H adjacent to P_j. Thus, Ω_j is a convex set, and each vertex P_j is contained in the interior of only one subdomain of the decomposition.

To prove the relations between MTP and SWR, we need a general result. The solution to the wave equation can be obtained by Huygens' principle [3] (Kirchhoff's formula in 3D [4]): *the solution at a point $P = (\mathbf{x}, t = \Delta T)$ depends only on the initial data on the closed ball $\overline{\mathcal{B}_{c\Delta T}(\mathbf{x})}$ of radius $c\Delta T$ and center $\mathbf{x}$ that is intersected by a cone drawn backward from P* (Fig. 1, left). Lemma 1 follows from this principle.

Lemma 1 *Consider the three-dimensional wave equation $\partial_{tt} u(\mathbf{x},t) = c^2 \Delta u(\mathbf{x},t)$ in $\Omega = \mathbb{R}^3$. Assume that the initial data $u(\mathbf{x},0) = g_0(\mathbf{x})$ and $\partial_t u(\mathbf{x},0) = g_1(\mathbf{x})$ are equal to 0 for all $\mathbf{x}$ in a convex polytope $\mathcal{P} \subset \mathbb{R}^3$, and 1 outside $\mathcal{P}$. Then, $u(\mathbf{x},t) = 0$ for all $(\mathbf{x},t)$ in a 4-dimensional polytope $\mathcal{Q}$ containing $\mathcal{P}$. The vertices of $\mathcal{Q}$ are located at $t = 0$ (the ones of $\mathcal{P}$) and at $t = R/(2c)$, where R is the radius of the largest ball contained in $\mathcal{P}$. Finally, at each time $t \in (0, R/(2c))$ the set of all points $(\mathbf{x},t)$ for $\mathbf{x} \in \mathcal{Q}$ is a polytope similar to $\mathcal{P}$.*

Proof. Consider a space-time point $(\mathbf{y},t)$. By Hyugens' principle (Kirchoff formula), $u(\mathbf{y},t) = 0$ if and only if $u(\mathbf{x},0) = 0$ and $\partial_t u(\mathbf{x},0) = 0$ for all $\mathbf{x}$ on $\overline{\mathcal{B}_{ct}(\mathbf{y})}$. Thus, $\mathcal{Q}$ can be constructed by rolling balls of different radii within $\mathcal{P}$ and applying Hyugens' principle. In particular, by rolling $\mathcal{B}_{ct}(\mathbf{y})$ within $\mathcal{P}$, we can obtain all $\mathbf{y} \in \Omega$ at time t such that $u(\mathbf{y},t) = 0$. Moreover, rolling $\mathcal{B}_{ct}(\mathbf{y})$ near $\partial\mathcal{P}$, meaning that $\overline{\mathcal{B}_{ct}(\mathbf{x})}$ touches $\partial\mathcal{P}$ without penetrating it, the trajectory drawn by the center $\mathbf{y}$ provides the boundary of a polytope similar to $\mathcal{P}$, and these points are all boundary points of $\mathcal{Q}$. The result follows by repeating the argument for all $t \in (0, R/(2c)]$. □

We can now prove precise relations between MTP and SWR.

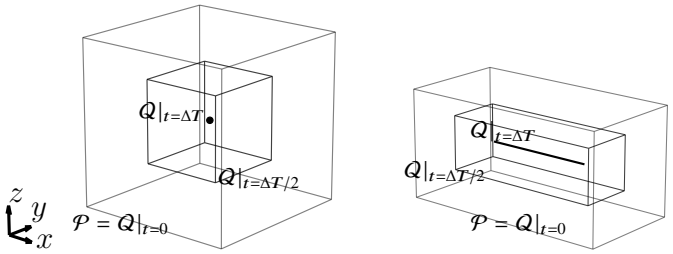

Fig. 2 Examples of applications of Lemma 1. **Left**: $\mathcal{P}$ is a cube of size $2R$. Rolling a sphere of radius $R/2$ one gets a smaller cube concentric with the initial one. When the sphere of radius R is considered, one gets only the barycenter of the initial cube. Thus, Q is a cube that shrinks to a point as t increases. **Right**: $\mathcal{P}$ is a rectangular parallelepiped. Rolling balls of increasing radii one gets rectangular parallelepipeds similar to the initial one and shrinking to a segment. Rolling balls of increasing radii one gets rectangular parallelepipeds similar to the initial one. The polytode Q shrinks to a segment as t increases.

Lemma 2 *Given a (continuous and piecewise linear) front $\mathcal{F}$ as the upper bound in time of a computed exact solution with vertices corresponding to the vertices of Ω_H. Consider a point P_j on $\mathcal{F}$ on which a new tent can be pitched. Then the tent $\mathcal{T}$ pitched in P_j is contained in the new portion of volume $\mathcal{V}$ of exact solution computed by a subdomain solve performed on the subdomain $Q_j = \Omega_j \times (0, T)$. In particular, $\mathcal{V}$ is also a polytope, and the vertex P'_j of $\mathcal{T}$ lies on the boundary of $\mathcal{V}$. If the mesh is regular and P_j coincides with the barycenter of Ω_j, then $\mathcal{T} = \mathcal{V}$.*

Proof. MTP pitches a new tent $\mathcal{T}$ (a convex polytope) by moving P_j along t till P'_j. Since we consider the wave equation with constant c, the new volume $\mathcal{V}$ of exact solution obtained by SWR on Q_j is a convex polytope by Lemma 1. Since $\mathcal{V}$ is not restricted to having a vertex corresponding to P_j, the subdomain solve can compute a volume $\mathcal{V}$ greater than $\mathcal{T}$ (and thus $\mathcal{T} \subseteq \mathcal{V}$). Hence, the result follows. □

Remark 1 The above assuMTPions and Lemma 1 say that for each vertex in Ω_H, where a tent is pitched, there is a subdomain problem capable of producing that tent.

Remark 2 Notice that the previous result states that a subdomain solve can compute a volume of the exact solution larger than the one of MTP. As an example consider Ω_j to be a 1D interval. Now, if P_j is the mid-point of Ω_j, then $\mathcal{T} = \mathcal{V}$. However, if P_j is different from the middle point, then $\mathcal{V}$ is larger than $\mathcal{T}$. See Fig. 1, right.

After this observation, one could think that SWR can advance faster than MTP, but this is not true. SWR exchanges information on the boundaries of the subdomains. Thus, if a larger volume of the exact solution is computed, a portion is not necessarily transmitted to the neighboring subdomains.

Theorem 1 *Assume that at the n-th iteration the MTP process pitches tents at the nodes whose indices are contained in $\mathcal{K}_n$. In other words, assume that the order used by MTP to select nodes where new tents are pitched is the same used by SWR to define the sequence of subdomain solves. Then MTP and SWR generate advancing fronts that are equal on the vertices of Ω_H.*

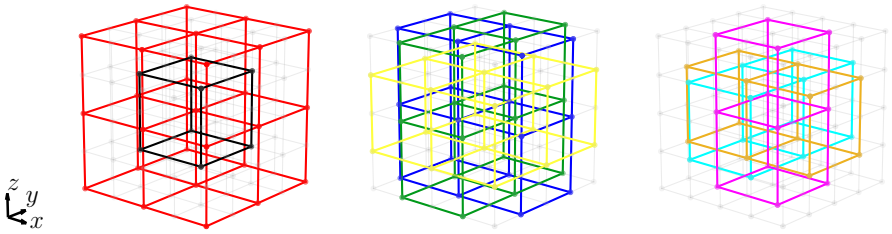

Fig. 3 **Left**: subdomains $\langle 000\rangle$ (red) and $\langle 111\rangle$ (black). **Middle**: subdomains $\langle 100\rangle$ (green), $\langle 010\rangle$ (blue), and $\langle 001\rangle$ (yellow). **Right**: subdomains $\langle 110\rangle$ (magenta), $\langle 011\rangle$ (orange), and $\langle 101\rangle$ (cyan).

Proof. The proof works by induction starting from the zero initial front and using Lemma 2 (and Remark 2) at each induction step. □

3 UTP: MTP by SWR in a 3D cube

We consider the space domain $\Omega = (0,1)^3$, and decompose it into overlapping subdomains $\Omega_j, \Omega = \cup_j \Omega_j$. To build them, we begin by a reference (non-overlapping) decomposition. First, we decompose the unit interval $(0,1)$ into N subintervals of length H: (x_{k-1}, x_k), for $k = 1, \ldots, N$, with $x_j = jH$. Then, the N^3 reference subdomains are defined as $(x_{k-1}, x_k)\times(x_{\ell-1}, x_\ell)\times(x_{m-1}, x_m)$, for $k, \ell, m = 1, \ldots, N$. We denote by $\langle 000\rangle$ the set of all indices corresponding to these N^3 subdomains, cf. Fig. 3, left. Starting from this reference set, we build

- three sets of $N^2(N-1)$ subdomains, whose indices form the sets $\langle 100\rangle$, $\langle 010\rangle$, and $\langle 001\rangle$, and which are obtained shifting the reference subdomains by $H/2$ in the direction x, y, and z, respectively (removing the last slice), see Fig. 3, middle;
- three sets of $N(N-1)^2$ subdomains, whose indices form the sets $\langle 110\rangle$, $\langle 011\rangle$, and $\langle 101\rangle$, and which are obtained shifting the reference subdomains by $H/2$ in the direction xy, yz, and xz, respectively (and removing the last slices), see Fig. 3, right;
- a set of $(N-1)^3$ subdomains, whose indices form the set $\langle 111\rangle$, and which is obtained shifting the reference subdomains by $H/2$ in the direction xyz (and removing the last slices), see Fig. 3, left.

The whole decomposition is the union of all these subdomain sets. All subdomains are cubes with edges of length H. Notice that the binary notation is used to easily identify a set: 0 means "as in the reference set", while 1 means "shifted", and the position indicates the direction. Notice also that we associate a different color to each subdomain set: $\langle 000\rangle$ is red, $\langle 111\rangle$ is black, $\langle 100\rangle$ is green, $\langle 010\rangle$ is blue, $\langle 001\rangle$ is yellow, $\langle 110\rangle$ is magenta, $\langle 011\rangle$ is orange, and $\langle 101\rangle$ is cyan; see Fig. 3.

The above decomposition induces naturally a mesh Ω_H discretizing Ω: This mesh is characterized by $M = (2N-1)^3$ vertices corresponding to all vertices of the subdomains and forming a uniform three-dimensional grid of size $H/2$. Essentially,

Algorithm 1 Staggered Unmapped Tent Pitching by SWR

Require: An initial guess function u^0 defined on $\Omega_H \times [0, T]$.

1: Set $n = 1$ and $v_j^0 = 0$ for $j = 1, \dots, M$ (all vertices of the mesh Ω_H).

2: **while** $\exists j \in \{1, \dots, M\} \ : \ v_j^{n-1} \neq T$ **do**

3: Set $\mathcal{K}_n = \begin{cases} \langle 000 \rangle & \text{if} \mod (n, 4) = 0, \\ \langle 001 \rangle \cup \langle 010 \rangle \cup \langle 100 \rangle & \text{if} \mod (n, 4) = 1, \\ \langle 011 \rangle \cup \langle 110 \rangle \cup \langle 101 \rangle & \text{if} \mod (n, 4) = 2, \\ \langle 111 \rangle & \text{if} \mod (n, 4) = 3. \end{cases}$

4: Compute the heights $v_j^n = \frac{H}{2c} + v_j^{n-1}$ for all $j \in \mathcal{K}_n$, and set $v_j^n = v_j^{n-1}$ for $j \notin \mathcal{K}_n$.

5: For each $j \in \mathcal{K}_n$ pitch a subdomain $\mathcal{T}_j := \Omega_j \times (v_j^{n-1}, v_j^n)$.

6: Solve the SWR subproblems (2) in $\mathcal{T}_j$, for all $j \in \mathcal{K}_n$, to get u_j^{n+1} in $\mathcal{T}_j$.

7: Update $u^0|_{\mathcal{T}_j} = u_j^{n+1}$ and $n = n + 1$.

8: **end while**

the subdomains correspond to cubic elements. Each of these elements has exactly one grid point in the interior (in its barycenter) where tents are pitched. Hence, this is a natural setting to study in detail the relation between MTP and SWR. A first observation is that the hypotheses of Section 2 are satisfied. Thus, assuming that the solution order condition of Theorem 1 holds, then MTP working on Ω_H is clearly equivalent to SWR. Now, our goal is to introduce an unmapped tent pitching method (UTP), and then accurately characterize the tents that the equivalent MTP would produce. To do so, we follow the approach of [2], where the space subdomains in 1D have been split into red (odd) and black (even) groups. This gives the solution order: starting from the red subdomains, the iterations consider alternatingly red and black subdomains. For our three-dimensional case, we consider a cycle of four steps: first, all $\langle 000 \rangle$ (red) subdomains are treated in parallel; second, all $\langle 100 \rangle$ (green), $\langle 010 \rangle$ (blue), and $\langle 001 \rangle$ (yellow) subdomains are treated in parallel; third, all $\langle 110 \rangle$ (magenta), $\langle 011 \rangle$ (orange), and $\langle 101 \rangle$ (cyan) subdomains are treated in parallel; fourth, all $\langle 111 \rangle$ (black) subdomains are treated in parallel. Differently from [2], and for ease of notation, we assume that on the subdomains one pitches rectangular tents with tent heights equal to $H/(2c)$. This corresponds to a so-called *staggered approach*[2]. The approach considered in [2] allows one to have different heights for the different colors, but requires more details for its definition and treatment. For this reason, we do not consider it in this short paper, and we defer its discussion to future work [1]. Our UTP scheme for the considered problem is formulated in Algorithm 1. In the same spirit of the UTP defined in [2], Alg. 1 computes the values v_j^n that correspond to the height of the advancing front at the n-th iteration on the (interior) vertices of Ω_H.

In a discrete setting, Alg. 1 is a space-time Restricted Additive Schwarz (XT-RAS) method, where at the n-th iteration only the subdomains whose indices are in $\mathcal{K}_n$ are solved. Notice also that Alg. 1 is a special case of UTP in a three-dimensional setting. One could generalize it using the usual MTP rules to define the sets $\mathcal{K}_n$

[2] The term staggered comes from the work [9], focusing on the construction of space-time meshes.

and the heights of the tent. Nevertheless, one can still code it in an XT-RAS form. However, this discussion is deferred to future work [1].

At this point, two simple questions arise: A) why and how does UTP Alg. 1 work? B) what kind of tents does it produce? To answer them, it is sufficient to study the first single cycle (the first four iterations of Alg. 1) running over the four cases defining the set $\mathcal{K}_n$ in Step 3. We will show that these four iterations compute the exact solution in $\overline{\Omega} \times [0, H/(2c)]$, and thus repeating them one solves (1) in $\overline{\Omega} \times [0, T]$.

Using the linearity of the problem, we can work on the error equations and set the data g_0 and g_1 in (1) to zero. Now, the idea is to compute for each subdomain group (red, green, blue, yellow, magenta, orange, cyan, and black) the space-time volume where zero initial data are propagated. This is obtained by applying Lemma 1 to a polytope that needs to be identified with care. Let us begin with a **red subdomain** $\langle 000 \rangle$. Here, only the initial data are zero, while the boundary data are not. Thus, we can apply Lemma 1 directly to the red subdomain, namely $\mathcal{P}$ is a cube corresponding to the red subdomain. It then follows that the space-time polytope where the zero data are propagated is a cube shrinking to a point at the barycenter of the cube. In particular, one can see that at time t the volume of zero data is again a cube with the same barycenter of the subdomain and edges of length $H - ct$. Moreover, for $t = H/(2c)$ one gets the ball of maximal radius that can be contained in the subdomain. Thus, at $t = H/(2c)$ the error is zero only at the barycenter of the cube. Denoting by $\mathbf{x}_b^R$ the barycenter of the considered red cube for $t = 0$, the space-time polytope we obtain is

$$\mathcal{R}_b = \mathbf{x}_b^R + \left\{(t, \mathbf{x}) \in \mathbb{R}^4 \,:\, t \in \left[0, \frac{H}{2c}\right],\ |x| \le \frac{H}{2c} - t,\ |y| \le \frac{H}{2c} - t,\ |z| \le \frac{H}{2c} - t\right\},$$

and is shown in Fig. 4, upper-left panel, where we clearly see a cube shrinking to a point. Here, the transparency of the red color indicates the time direction: the darker the color, the larger the value of t. Let us now consider a **green subdomain** $\langle 100 \rangle$. Since the corresponding subdomain problem takes zero values from the two neighboring red subdomains, we can apply Lemma 1 to the polytope $\mathcal{P}$ obtained as the union of the two neighboring red subdomains (see Fig. 5, left), and then restricting the result to the original green cube. In particular, the space-time polytope $\mathcal{Q}$ obtained from Lemma 1 applied to the union of the two red subdomains is exactly the one shown in Fig. 2 (right). However, this needs to be restricted only to points $(\mathbf{x}, t)$ being the vertices of Hyugens' cones whose balls at $t = 0$ are centered at points $\mathbf{x}$ in the green cube. If $\mathbf{x}_b^G$ is the barycenter of the green cube, we get

$$\mathcal{G}_b = \mathbf{x}_b^G + \left\{(\mathbf{x}, t) \in \mathbb{R}^4 \,:\, t \in \left[0, \frac{H}{2c}\right],\ |x| \le \frac{H}{2c},\ |y| \le \frac{H}{2c} - t,\ |z| \le \frac{H}{2c} - t\right\},$$

which is shown in Fig. 4, middle-left panel. In this case, the cube shrinks to a segment parallel to the x-axis and of length $H/(2c)$. **Blue** $\langle 010 \rangle$ and **yellow** $\langle 001 \rangle$ **subdomains** can be treated similarly. If $\mathbf{x}_b^B$ and $\mathbf{x}_b^Y$ denote their barycenters, we get

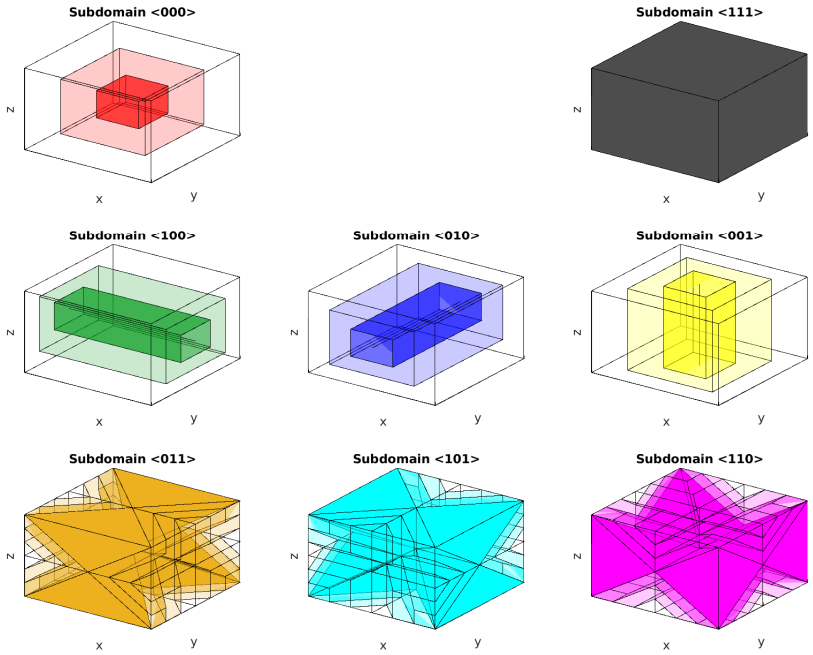

Fig. 4 Volumes (space-time polytopes) of exact solution computed on the different subdomains.

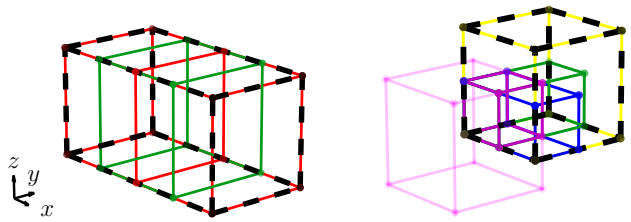

Fig. 5 **Left**: The black dashed line represents the union of the two red subdomains neighboring a green one. **Right**: The black dashed line is the polytope (the yellow cube) where Lemma 1 must be applied for the magenta subdomain.

$$\mathcal{B}_b = \mathbf{x}_b^B + \left\{(\mathbf{x},t) \in \mathbb{R}^4 \,:\, t \in \left[0, \frac{H}{2c}\right],\ |x| \le \frac{H}{2c} - t,\ |y| \le \frac{H}{2c},\ |z| \le \frac{H}{2c} - t\right\},$$
$$\mathcal{Y}_b = \mathbf{x}_b^Y + \left\{(\mathbf{x},t) \in \mathbb{R}^4 \,:\, t \in \left[0, \frac{H}{2c}\right],\ |x| \le \frac{H}{2c} - t,\ |y| \le \frac{H}{2c} - t,\ |z| \le \frac{H}{2c}\right\},$$

which are shown in Fig. 4, middle-middle and middle-right panel, respectively. Let us now consider a more subtle case: the **magenta subdomain** $\langle 110 \rangle$. The corresponding subproblem takes zero values from green, blue, and yellow subdomains. However, we cannot take the union of all neighboring green, blue, and yellow subdomains, because the boundary values on the vertical faces of the yellow subdomains (aligned

with the red ones) are not correct, and thus cannot be penetrated by the rolling spheres. The trick is to split the magenta cube into eight smaller cubes of size $H/2$ and treat them separately. For each of these smaller cubes the actual volume where the balls can be rolled is the union of the yellow subdomain and portions of blue and green subdomains, as shown in Fig. 5 (right). This coincides with the yellow cube. Thus, we can apply Lemma 1 to $\mathcal{P}$ being the yellow cube (giving again a cube shrinking to a point as in Fig. 2) and then restrict the result to Huygens' cones of balls at $t = 0$ with centers lying in the small magenta cubes. In this way, the center of the shrinking cube (namely, the barycenter of the yellow cube) coincides with the corner of the small magenta cube. Therefore, denoting by $\mathbf{x}_b^M$ the barycenter of the magenta cube, and assuming that we are looking at the small magenta cube corresponding to $\mathbf{x}_b^M + [-H/2, 0]^3$, the obtained polytope is

$$\mathcal{M}_b^{---} = \mathbf{x}_b^M + \left\{(\mathbf{x}, t) \,:\, t \in \left[0, \frac{H}{2c}\right],\, \mathbf{x} \in \left[-\frac{H}{2}, 0\right]^3,\, x - z \le \frac{H}{2c} - t,\, y - z \le \frac{H}{2c} - t\right\}.$$

If we repeat the same argument for all the other seven cubes and use the notation $\mathcal{I}^+ := [0, H/2]$ and $\mathcal{I}^- := [-H/2, 0]$, we obtain, for example,

$$\mathcal{M}_b^{-+-} = \mathbf{x}_b^M + \left\{(\mathbf{x}, t) \,:\, t \in \left[0, \frac{H}{2c}\right],\, \mathbf{x} \in \mathcal{I}^- \times \mathcal{I}^+ \times \mathcal{I}^-,\, x - z \le \frac{H}{2c} - t,\, -y - z \le \frac{H}{2c} - t\right\},$$

$$\mathcal{M}_b^{+++} = \mathbf{x}_b^M + \left\{(\mathbf{x}, t) : t \in \left[0, \frac{H}{2c}\right], \mathbf{x} \in \mathcal{I}^+ \times \mathcal{I}^+ \times \mathcal{I}^+, -x + z \le \frac{H}{2c} - t, -y + z \le \frac{H}{2c} - t\right\},$$

and we omit the others for brevity. Thus, we obtain

$$\mathcal{M}_b = \mathcal{M}_b^{---} \cup \mathcal{M}_b^{+--} \cup \mathcal{M}_b^{-+-} \cup \mathcal{M}_b^{--+} \cup \mathcal{M}_b^{++-} \cup \mathcal{M}_b^{-++} \cup \mathcal{M}_b^{+-+} \cup \mathcal{M}_b^{+++}.$$

This volume is shown in Fig. 4 (bottom right). The **orange** $\langle 101 \rangle$ and **cyan** $\langle 011 \rangle$ **subdomains** can be treated similarly. They are shown in Fig. 4 (bottom left and bottom middle). Finally, consider a **black subdomain** $\langle 111 \rangle$. In this case, the corresponding subproblem gets correct zero data on all the boundaries. Thus, the volume of propagated zero error coincides with the considered cube at every time t. Hence, denoting by $\mathbf{x}_b^B$ the barycenter of the black cube, we have (see Fig. 4, top right)

$$\mathcal{B}_b = \mathbf{x}_b^B + \left\{(\mathbf{x}, t) \,:\, t \in \left[0, \frac{H}{2c}\right],\, \mathbf{x} \in \left[-\frac{H}{2}, \frac{H}{2}\right]\right\}.$$

This means that all black subdomains are resolved exactly for all times in $[0, H/(2c)]$. Thus, the UTP Alg. 1 solved exactly (1) for $t \in [0, H/(2c)]$ with the first four iterations.[3] Performing four more iterations and repeating exactly the same above arguments, one can solve the problem for all times $t \in [H/(2c), 2H/(2c)]$. Continuing in this way, Alg. 1 can solve the problem for all times $t \in [0, T]$.

[3] Notice that we did not discuss the behavior near the boundary of $\Omega = (0, 1)^3$. Here, the other colors compute the exact solution before the final black iteration, as we will show in [1].

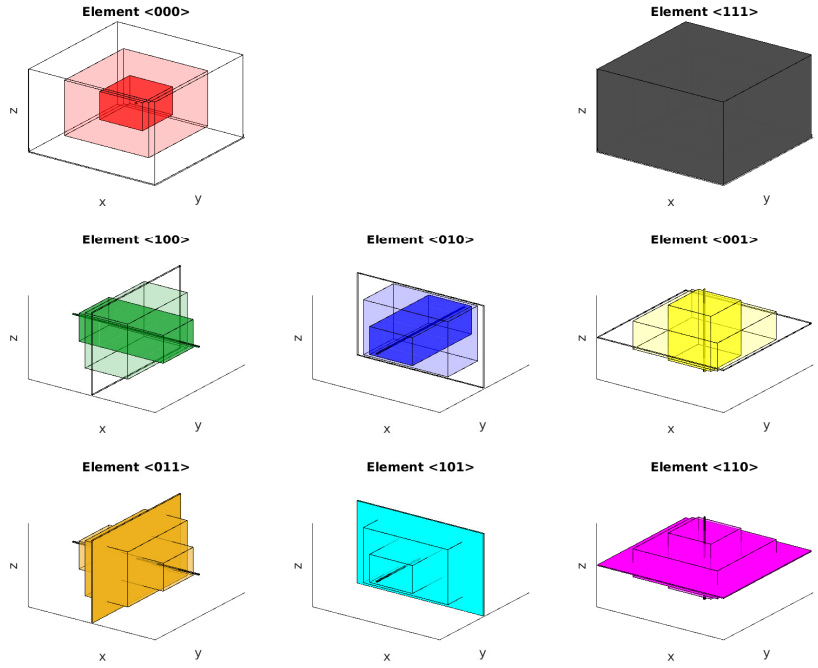

Fig. 6 Elements (space-time polytopes) computed by UTP on the subdomains and corresponding to those of MTP.

So far, we focused on the behavior of the UTP Alg. 1 and its convergence. Now, we focus on its relations to MTP and build precisely the elements that MTP would construct. To do so, we can use Theorem 1, which implies that the elements of MTP can be obtained by removing from the volumes of computed exact solution in each subdomain, the volume of exact solution computed at the previous iterations in the neighboring subdomains. We begin with the **red subdomains**. Here, since there is nothing to remove, the MTP elements $\mathcal{R}_b^E$ coincide with the volumes of exact solution: $\mathcal{R}_b^E = \mathcal{R}_b$. This element is shown in the top-left panel of Fig. 6. Let us now consider the **green subdomains**. We need to remove from the interior of $\mathcal{G}_b$ the portions of the interior of $\mathcal{R}_b$ corresponding to the two red subdomains neighboring the green one, and take the closure of the set obtained. This process is shown in Fig. 7. At $t = 0$, subtracting the two open red cubes from the green open cube, one gets a square parallel to the yz plane and lying between the two red cubes. This square becomes a segment when projected onto the xy plane (see the left panel of Fig. 7). When t increases the two red cubes shrink toward a point, leaving room for the green element. Here, only the two intersections of the shrank red cubes with the green volume must be removed (see the middle panel of Fig. 7). Finally, at time $t = H/(2c)$, the two red cubes become two points and the green segment (parallel to the x axis) remains unchanged. The process we just described corresponds to adding

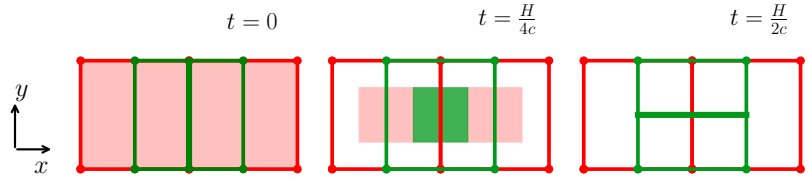

Fig. 7 Space-time elements of a green subdomain and of the two neighboring red subdomains.

the constraint $|x| \leq t$ for $t \in \left[0, \frac{H}{2c}\right]$ to the ones characterizing the set $\mathcal{G}_b$. Hence, the green element $\mathcal{G}_b^E$ is

$$\mathcal{G}_b^E = \mathbf{x}_b^G + \left\{(\mathbf{x}, t) \in \mathbb{R}^4 \,:\, t \in \left[0, \frac{H}{2c}\right],\ |x| \leq t,\ |y| \leq \frac{H}{2c} - t,\ |z| \leq \frac{H}{2c} - t\right\}.$$

Thus, the green element evolves in time starting from a plane to a segment; see the middle-left panel of Fig. 6. One can treat **blue and yellow subdomains** in a similar manner, the corresponding MTP elements are

$$\mathcal{B}_b^E = \mathbf{x}_b^B + \left\{(\mathbf{x}, t) \in \mathbb{R}^4 \,:\, t \in \left[0, \frac{H}{2c}\right],\ |x| \leq \frac{H}{2c} - t,\ |y| \leq t,\ |z| \leq \frac{H}{2c} - t\right\},$$
$$\mathcal{Y}_b^E = \mathbf{x}_b^Y + \left\{(\mathbf{x}, t) \in \mathbb{R}^4 \,:\, t \in \left[0, \frac{H}{2c}\right],\ |x| \leq \frac{H}{2c} - t,\ |y| \leq \frac{H}{2c} - t,\ |z| \leq t\right\},$$

see the middle-middle and middle-right panels of Fig. 6. Let us now focus on the **magenta subdomain**: to obtain the magenta element $\mathcal{M}_b^E$, we must remove from the magenta volume $\mathcal{M}_b$ the intersections of $\mathcal{M}_b$ with the neighboring green, blue and yellow volume. This process is shown in Fig. 8. At $t = 0$, removing the interior of the green, blue and yellow volumes from the magenta one leads to a segment parallel to the z axis. When t increases, the green, blue and yellow volume shrink toward segments and leave room to the magenta element, that at $t = \frac{H}{4c}$ is a cube and evolves toward a square parallel to the xy plane. This is also shown in Fig. 6 (bottom-right panel) and corresponds to adding the constraints $|x| \leq t$ and $|y| \leq t$ to the ones used to define $\mathcal{M}_b$. A direct inspection reveals that the element $\mathcal{M}_b^E$ has the form

$$\mathcal{M}_b^E = \mathbf{x}_b^M + \left\{(\mathbf{x}, t) \,:\, t \in \left[0, \frac{H}{2c}\right], \mathbf{x} \in \left[-\frac{H}{2}, \frac{H}{2}\right]^3,\ |x| \leq t,\ |y| \leq t, |z| \leq \frac{H}{2c} - t\right\},$$

as shown in Fig. 6 (bottom-right panel). All other elements on **orange, cyan, and black subdomains** can be obtained in the same way. Notice that the black element works in the opposite manner of the red one: it evolves from a point to a cube. All these elements are shown in Fig. 6, but we defer their algebraic forms to a future and more extensive work [1] for the sake of brevity.

To conclude, we explored for the first time in 3D the relations between SWR, MTP and UTP (in their staggered versions) and proved their equivalence in terms of advancing fronts. This analysis allowed us to precisely characterize the tents that MTP would compute on a simple uniform mesh of cubic elements discretizing the

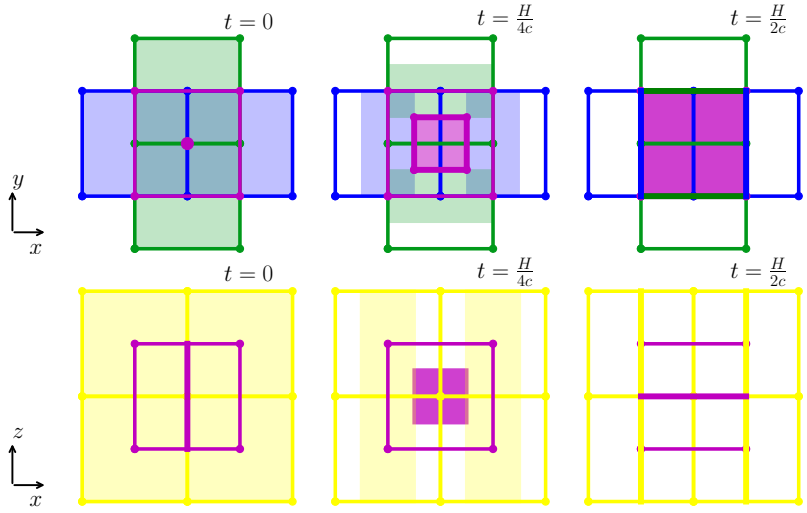

Fig. 8 Space-time magenta elements and volumes of the neighboring green, blue, and yellow subdomains.

unit cube. Even in this very simple 3D geometric setting, the tents are complicated 4D polytopes, and the advantage of UPT becomes evident, where the "tents" considered are simply cubes.

References

1. G. Artoni, A. Ciaramella, M.J. Gander, and I. Mazzieri. Space-time RAS methods for wave-propagation problems. *in preparation*, 2024.
2. G. Ciaramella, M.J. Gander, and I. Mazzieri. Unmapped tent pitching schemes by waveform relaxation. In *Domain Decomposition Methods in Science and Engineering XXVII*, pages 455–462, Cham, 2024. Springer Nature Switzerland.
3. R. Courant and D. Hilbert. *Methods of Mathematical Physics: Volume II (Partial differential equations)*. Wiley Classics Edition. John Wiley and Sons, 1989.
4. L.C. Evans. *Partial Differential Equations*. Graduate studies in mathematics. American Mathematical Society, 1998.
5. Martin J. Gander and Laurence Halpern. Absorbing boundary conditions for the wave equation and parallel computing. *Mathematics of computation*, 74(249):153–176, 2005.
6. Martin J. Gander, Laurence Halpern, and Frédéric Nataf. Optimal Schwarz waveform relaxation for the one dimensional wave equation. *SIAM Journal on Numerical Analysis*, 41(5):1643–1681, 2003.
7. Martin J. Gander and Thibaut Lunet. *Time Parallel Time Integration*. SIAM, 2024.
8. J. Gopalakrishnan, J. Schöberl, and C. Wintersteiger. Mapped tent pitching schemes for hyperbolic systems. *SIAM J. Sci. Comput.*, 39(6):B1043–B1063, 2017.
9. R.B Lowrie. Compact higher-order numerical methods for hyperbolic conservation laws. *PhD thesis, University of Michigan*, 1996.
10. Alper Üngör and Alla Sheffer. Pitching tents in space-time: Mesh generation for discontinuous Galerkin method. *International Journal of Foundations of Computer Science*, 13(02):201–221, 2002.

MOX Technical Reports, last issues

Dipartimento di Matematica
Politecnico di Milano, Via Bonardi 9 - 20133 Milano (Italy)

54/2024 Antonietti, P.F.; Botti, M.; Cancrini, A.; Mazzieri, I.
A polytopal discontinuous Galerkin method for the pseudo-stress formulation of the unsteady Stokes problem

53/2024 Caldana, M.; Hesthaven, J. S.
Neural ordinary differential equations for model order reduction of stiff systems

Negrini, G.; Parolini, N.; Verani, M.
An Immersed Boundary Method for Polymeric Continuous Mixing

52/2024 Botti, M.; Mascotto, L.
A Necas-Lions inequality with symmetric gradients on star-shaped domains based on a first order Babuska-Aziz inequality

51/2024 Antonietti, P.F.; Corti, M.; Lorenzon, G.
A discontinuous Galerkin method for the three-dimensional heterodimer model with application to prion-like proteins' dynamics

50/2024 Fumagalli, I.; Parolini, N.; Verani, M.
A posteriori error analysis for a coupled Stokes-poroelastic system with multiple compartments

49/2024 Ballini, E.; Formaggia, L.; Fumagalli, A.; Keilegavlen, E.; Scotti, A.
A hybrid upwind scheme for two-phase flow in fractured porous media

Ballini, E.; Formaggia, L.; Fumagalli, A.; Keilegavlen, E.; Scotti, A.
A hybrid upwind scheme for two-phase flow in fractured porous media

48/2024 Cicalese, G.; Ciaramella, G.; Mazzieri, I.
Addressing Atmospheric Absorption in Adaptive Rectangular Decomposition

47/2024 Franco, N.R.; Brugiapaglia, S.
A practical existence theorem for reduced order models based on convolutional autoencoders